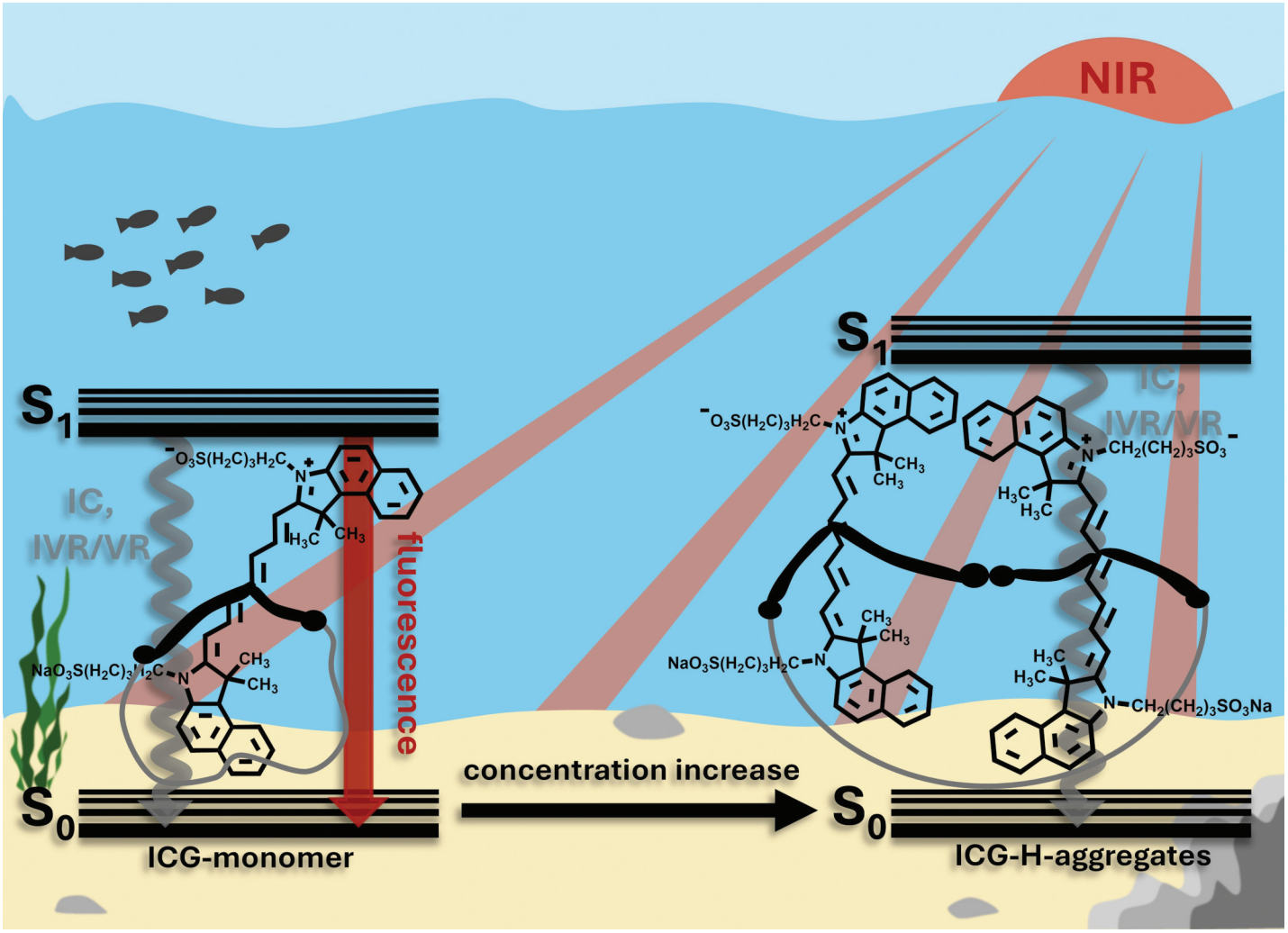

Showcasing research from Professor Andreas-Neil Unterreiner's laboratory, Institute of Physical Chemistry, Karlsruhe Institute of Technology, Germany.

ICG revisited: excited-state dynamics as a function of dye concentration and solvent environment

This study revisits the excited-state dynamics of indocyanine green (ICG), showing how solvent and concentration influence its photophysical behaviour. Concentration-dependent formation of H-aggregates in aqueous solution alters both steady-state and time-resolved properties, reducing fluorescence quantum yield and promoting non-radiative decay. By disentangling monomeric and aggregated spectral signatures, the work lays a foundation for understanding ICG in nanocluster systems—bridging spectroscopy with photothermal and biomedical applications.

Image reproduced by permission of Maria T. Lahm and Andreas-Neil Unterreiner from *Dalton Trans.*, 2025, **54**, 15406.

As featured in:

See Andreas-Neil Unterreiner *et al.*, *Dalton Trans.*, 2025, **54**, 15406.

ROYAL SOCIETY OF CHEMISTRY

rsc.li/dalton

Registered charity number: 207890

Dalton Transactions

ROYAL SOCIETY OF CHEMISTRY

PAPER

View Article Online
View Journal | View Issue

Cite this: *Dalton Trans.*, 2025, **54**, 15406

ICG revisited: excited-state dynamics as a function of dye concentration and solvent environment

Maria T. Lahm,[a] Pascal Rauthe,[a] Kai-Ching Fan,[b] Claus Feldmann [b] and Andreas-Neil Unterreiner *[a]

Indocyanine green (ICG) is a clinically approved tricarbocyanine dye widely used in medical imaging and photodynamic therapy. Its incorporation into inorganic hybrid nanoparticles (IOH-NPs) offers a highly promising strategy for the targeted delivery of therapeutic agents, particularly in photothermal applications. Despite extensive use of ICG, the influence of solvent and concentration on its excited-state behaviour remains incompletely understood, but an in-depth understanding of these photophysical properties is essential for elucidating its functional role within the IOH-NPs. Therefore, this study combines steady-state and time-resolved spectroscopic methods to examine the dependence of the excited-state dynamics of the first excited singlet state of ICG on both solvent environments and dye concentration. The photophysical behaviour of ICG was characterised in ethanol (EtOH), dimethyl sulfoxide (DMSO) and demineralised water across a systematically varied concentration range from 0.08 to 100 μM. The steady-state absorption behaviour of ICG in EtOH and DMSO largely showed a concentration independence, whereas in water, concentration-dependent H-aggregation was observed. The fluorescence quantum yield (fQY) decreased with increasing dye concentration above approximately 0.2 μM, beginning from approximately 22% in EtOH, 42% in DMSO and 5% in water. The time-resolved studies were conducted by time-correlated-single-photon-counting (TCSPC) at λ_{ex} = 366 nm and transient-absorption spectroscopy using femtosecond laser pulses at λ_{ex} = 800 nm. Relaxation from the first excited singlet state of ICG occurs on timescales of 500–600 ps in EtOH, 700–900 ps in DMSO and 120–160 ps in water, reflecting increased nonradiative decay in aqueous solution. In EtOH and DMSO, excited-state dynamics remained largely concentration-independent, while in water aggregation effects became more pronounced at higher concentration. A clear correlation between excited-state lifetime and fQY was observed across all solvents.

Received 8th August 2025,
Accepted 29th September 2025

DOI: 10.1039/d5dt01894c

rsc.li/dalton

Introduction

Nanocarrier-based delivery systems (NPs, nanoparticles) are a powerful strategy for targeted therapeutic applications in chemical and biological systems due to their ability to combine high biocompatibility and simple design using components with established clinical approval.[1,2] In 2022, our group[3] demonstrated the feasibility of temporally and spatially confined photothermal heat transfer – on the nm scale and on a timescale of hundreds of picoseconds (ps) – *via* photo-induced polymerization using gold nanorods excited at 800 nm by femtosecond (fs) laser pulses.[3] Further polymerization studies[4] demonstrated that photoexcited dyes, such as indocyanine green (ICG) (Fig. 1) – a polymethine dye approved for clinical use by both the U.S. Food and Drug Administration (FDA) and the European Medicines Agency (EMA) – can also function as efficient heat transducers.[5–8] Given its strong absorption and emission in the near-infrared (NIR) region around 800 nm,[6,7] ICG is particularly well-suited for biological applications, as this spectral window (700–1000 nm) permits tissue penetration of several cm.[8–14] Its potential in medical applications, *e.g.* in phototheranostics, has been compellingly demonstrated.[15] However, several molecular limitations constrain its clinical application, including chemical instability in aqueous and physiological environments[2,6] and poor *in vivo* photostability.[2,16] Incorporating ICG into nanocarriers can

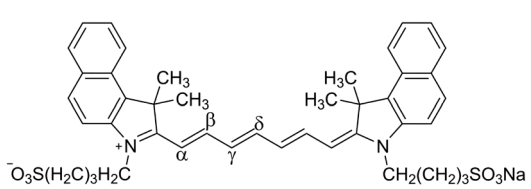

Fig. 1 Molecular structure of the all-*trans* isomer of indocyanine green (ICG, benzoindotricarbocyanine, $C_{43}H_{47}N_2NaO_6S_2$).

[a]*Karlsruhe Institute of Technology, Institute of Physical Chemistry, 76131 Karlsruhe, Germany. E-mail: andreas.unterreiner@kit.edu*
[b]*Karlsruhe Institute of Technology, Institute of Inorganic Chemistry, 76131 Karlsruhe, Germany*

mitigate these drawbacks by shielding the molecule from environmental influences and enabling precise, light-triggered activation at the target site, thereby improving both its suitability and specificity for therapeutic applications.[8,17–19] The photothermal effect of ICG arises from its efficient relaxation *via* internal conversion (IC), converting part of the absorbed photon energy into heat.[20,21] As aggregated ICG-species exhibit higher quantum yield of IC compared to the monomer,[14,21] and NPs are known to promote aggregation of ICG molecules,[7] ICG-containing NPs show great promise for photothermal applications, including photothermal therapy (PTT).[5–8] One such system consists of $[GdO]^+[ICG]^-$-NPs, which are classified as inorganic, sulfonate-based hybrid NPs (IOH-NPs).[2,16,22–24] Given that aggregation significantly alters the optical and excited-state properties of ICG,[7,15,25] a throughout understanding of the excited-state dynamics of the aggregates compared to the monomer under varying environmental conditions is prerequisite for investigating its photophysical behaviour and thereby its functional role within NPs,[7] as these properties strongly depend on both solvent environment and dye concentration.[5,15,25–28] Aqueous solution provides an ideal model system for this purpose, as ICG undergoes concentration-dependent H-aggregation in highly polar solvents at elevated concentrations.[7,26,27,29,30] ICG is known to form non-covalently bound dimers in water at concentrations ranging from approximately 3×10^{-8} to 10^{-4} mol L^{-1}, with higher-order oligomers emerging above 0.1 mM.[27] To distinguish the dynamics of aggregated ICG from those of the monomer, we conducted systematic investigations of the excited-state dynamics of the first excited singlet state of ICG in condensed phase across a controlled dye-concentration range in demineralised water and non-aggregating reference media, namely ethanol (EtOH) and dimethylsulfoxide (DMSO).[31–33] By covering a concentration range of 0.08 to 100 μM and using complementary spectroscopic techniques, our study enables continuous monitoring of the progression of aggregation in water and allows a comprehensive examination of concentration-dependent aggregation effects on its excited-state dynamics. Steady-state spectroscopic measurements were performed using absorption and fluorescence spectroscopy, while time-resolved techniques included time-correlated single-photon counting (TCSPC) and transient-absorption spectroscopy with fs-laser pulses at λ_{ex} = 800 nm. Due to its physiological compatibility, water serves as an optimal medium for substances intended for biomedical applications. Temperature also affects the properties of ICG, for example by accelerating its degradation at elevated temperatures or promoting aggregate formation.[7,33,34] To minimise temperature-induced effects on the behaviour of ICG, all spectroscopic measurements were performed at room temperature.

Results and discussion

Steady-state absorption and fluorescence behaviour

The steady-state absorption behaviour of ICG was investigated at concentrations from 0.08 up to 100 μM. In EtOH and DMSO, the spectra exhibited similar band shapes across this concentration range (Fig. 2(a), Fig. S1(a)), indicating negligible aggregation tendency due to strong solvation of ICG.[26,27] The main absorption band of the ICG monomer[26,34,35] varied slightly with solvent polarity, appearing at ~778 nm in water, 787 nm in EtOH and 795 nm in DMSO (Fig. 2). Consistent with the findings of J. Zhou *et al.*[36] and De Boni *et al.*,[37] this band was assigned to the π–π* transition from the lowest vibrational level ν_0 of the electronic ground state S_0 to the lowest vibrational level ν_0' of the first excited singlet state S_1. A vibronic shoulder appeared at ~728 nm in EtOH, at ~733 nm in DMSO and at ~718 nm for concentrations up to ~2 μM in water, corresponding to blue shifts of ~1030 cm^{-1}, ~1064 cm^{-1} and ~1074 cm^{-1} relative to the main band, respectively, and was attributed to a vibrational progression.[36,38] Aggregation of ICG in water influenced both the shape and position of the absorption maxima. Starting at concentrations between 2 and 3 μM, an additional absorption maximum emerged at 713 nm, overlapping the shoulder at 718 nm and identified as the main absorption band of the ICG dimer.[5,26,30] With increasing ICG concentration, the monomer band diminished in favour of hypsochromically shifted aggregate bands, resulting in deviations from Beer–Lambert law behaviour (Fig. S2). According to Chon *et al.*[26] H-aggregates and monomers coexist in approximately equal proportions at an ICG concentration of 50 μM. At 100 μM, the absorption band of the H-aggregates exceeded that of the monomers in intensity. Oligomeric ICG aggregates predominantly absorb

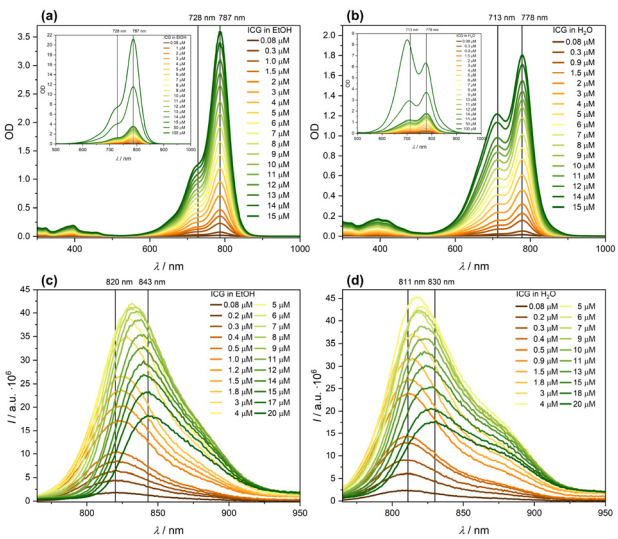

Fig. 2 Stationary absorption spectra of ICG in (a) EtOH and (b) water in a concentration range of 0.08 to 100 μM. Path length 1 mm (c(ICG) = 0.08–15 μM), 1 cm (c(ICG) = 50, 100 μM). The experimental data for the 50 and 100 μM solutions were multiplied by a factor of 10 for plotting purposes. The vertical lines indicate the absorption maxima of the ICG monomer or dimer and the vibronic shoulder. Stationary emission spectra of ICG in (c) EtOH and (d) water as a function of concentration in the range of 0.08 to 20 μM. Path length 1 cm. The vertical lines indicate the emission maxima corresponding to low ICG concentrations up to 0.3 μM and to higher ICG concentrations of 20 μM.

near 700 nm,[26,27,34,35] explaining the hypsochromic shift of the absorption maximum from 778 nm by 1392 cm^{-1} to 702 nm (c_{ICG} = 100 μM), which was attributed to enhanced aggregation. Higher oligomers and J-aggregates, which are reported to form exclusively at concentrations above 100 μM and exhibit an absorption maximum at around 890 nm,[26,27,39,40] were not observed up to 100 μM and are therefore expected to be negligible.

Although ICG is among the most widely used standards for NIR fluorescence quantum yield (fQY) measurements, the values reported – according to a foundational study by Benson *et al.*[41] – should be considered as general trends rather than precise references for comparing individual dyes.[41–43] Reported fQYs of ICG vary across different publications, *e.g.* ranging from 12%[44] to 21%[42] in DMSO, from 5%[45] to 13%[43] in EtOH and from 1%[45] to 2.7%[27] in water. To minimise uncertainty, a comprehensive concentration-dependent study of the fQY of both the reference systems and ICG in EtOH, DMSO and water was conducted following the protocol by Resch-Genger *et al.*,[46] covering a finely spaced concentration series from 0.08 to 20 μM to evaluate quenching effects. The use of literature data acquired at defined concentrations for the reference standards was essential, given that concentration-dependent effects on emission behaviour have also been demonstrated for both chosen standards HITCI and IR-820 (Fig. S6, Tables S1 and 2). The detailed experimental procedure is described in the section Materials and methods. The accuracy of the setup was estimated to be better than 2% by referencing the literature-reported fQY of IR-820 at a defined dye concentration against HITCI (SI).

The emission maxima of ICG displayed a slight blue shift with increasing solvent polarity, appearing at 820 nm in EtOH, 829 nm in DMSO and 811 nm in water for low concentrations up to 0.3 μM (Fig. 2(c, d), and Fig. S1(b)). As the emission band around 800 nm corresponds to the energy gap between the first excited singlet state S_1 and the ground state S_0 of the ICG monomer,[36,37] the emission was attributed to a transition from the lowest vibrational level of S_1 to a vibrational level of S_0. ICG displayed a Stokes shift of about 585 cm^{-1} in EtOH (c_{ICG} = 1.2 μM), 588 cm^{-1} in DMSO (c_{ICG} = 1.2 μM) and 538 cm^{-1} in water (c_{ICG} = 1.5 μM) (Fig. S7). In all three solvents, the fluorescence spectra of ICG showed a shoulder on the bathochromic side of the emission maximum, which was more pronounced in the more polar solvents EtOH and water compared to DMSO (Fig. 2(c, d), and Fig. S1(b)). The energy difference between the shoulder and the principal maximum in the steady-state fluorescence spectra (~1000–1024 cm^{-1} for c_{ICG} = 1.2 μM in EtOH and DMSO and c_{ICG} = 1.5 μM in water) closely matched that between the hypsochromic shifted shoulder and the main absorption band in the corresponding steady-state absorption spectra (1030 cm^{-1} in EtOH, 1064 cm^{-1} in DMSO, 1074 cm^{-1} in water), indicating a vibrational progression of the monomer. The comparable vibrational structures and symmetries of the electronic ground and excited states suggest that the absorption and emission spectra should, in principle, appear as mirror images.[26] Given that the energy difference between the absorption maxima of the H-aggregates and the ICG monomer in water (1392 cm^{-1}) substantially exceeded the energy gap between the bathochromic shoulder and the emission maximum, an assignment to the dimeric form of ICG was excluded.

With increasing concentration, the emission maximum showed a bathochromic shift of approximately 300 cm^{-1} in all three tested solvents – consistent with literature reports[10,32] – reaching 843 nm in EtOH, 851 nm in DMSO and 830 nm in water at 20 μM (Fig. 2(c, d), and Fig. S1(b)). As reabsorption effects are known to induce a concentration-dependent red-shift in fluorescence without significantly affecting the absorption spectra,[46] fluorescence quenching was assumed to begin at concentrations around 0.2–0.3 μM in the experimental data. Applying the reabsorption correction to the emission spectra using eqn (3) and (4) (Fig. S3–S5) confirmed that quenching started at this dye concentration. In this study, fQY values were derived from emission spectra without applying reabsorption correction, thereby underscoring the critical importance of concentration dependence in determining fQY, particularly for NIR dyes. The results at defined ICG concentrations were in agreement with literature values, such as approximately 13% in EtOH for a 5 μM solution reported by Rurack *et al.*[43] and about 3.5% in water for a 0.3 μM solution reported by Hoshi *et al.*,[47] highlighting the necessity of strictly defined concentration conditions when comparing values across different studies. At ICG concentrations where reabsorption effects are not expected to occur ($c_{ICG} \leq 0.2$ μM), the fQy was determined to be ~22% in EtOH, ~42% in DMSO and ~5% in water. Accordingly, the fQY of ICG in water was 4–5 times lower than in EtOH and nearly 9 times lower than in DMSO. Since solvents containing functional groups with high-energy vibrations (*e.g.* OH groups) are known to act as potent quenchers of dye fluorescence, especially for those absorbing and emitting beyond 600 nm,[48] it is not unexpected that the fQY of ICG decreases progressively from DMSO to EtOH and finally to water. With increasing concentration, the bathochromic shift of the emission maxima in the steady state fluorescence spectra was accompanied by fluorescence quenching, as evidenced by a simultaneous decrease in fQY to ~4% in EtOH, ~10% in DMSO and below 1% in water at c_{ICG} = 20 μM (Tables S3–S8). According to the studies by Chon *et al.*[26] and Philip *et al.*[27] the fluorescence emission of ICG originates predominantly from its monomeric form and decreases with increasing H-aggregation. These H-aggregates act as non-emissive quenching centres by reducing monomer fluorescence *via* energy transfer between excited and non-excited molecules.[27] Consequently, the fluorescence of ICG in water is additionally modulated by concentration-dependent aggregation phenomena.[35]

Time-resolved absorption and fluorescence behaviour

The electronic relaxation behaviour of ICG was investigated by time-resolved transient-absorption spectroscopy in the concentration range of 10 to 100 μM with particular attention to concentration-dependent effects and variations in solvent environment. The results were complemented by steady-state spectro-

scopic data and TCSPC measurements (Fig. S12). Pump-induced changes of the optical density (ΔOD) at concentrations below 10 μM were insufficient for reliable time-resolved analysis, a limitation that was most pronounced in aqueous solutions.

ICG demonstrated concentration-dependent dynamics in aqueous solution. Since no aggregation was detected in EtOH or DMSO within the investigated concentration range by steady-state spectroscopy, the monomer dynamics in these solvents served as references (SI). The transient absorption spectra (TAS) of ICG (c_{ICG} = 10 μM) in aqueous solution featured a positive transient response spanning the probe range from approximately 400 to 646 nm, which appeared within less than 100 fs after photoexcitation, over roughly 12 ps and subsequently decayed over increasing delay times, disappearing completely after about 500 ps (Fig. 3(a)). This positive transient response showed an intensity maximum near 570 nm with a hypsochromic shoulder at 476 nm and was attributed to singlet excited-state absorption (ESA), based on its consistency with transient-absorption data obtained in EtOH and DMSO (SI) and agreement with previously reported results.[15] An isosbestic point at ΔmOD = 0 emerged around 12 ps after photoexcitation at approximately 646 nm and persisted until the transient response had fully decayed. Within the first 12 ps, the individual transients converged toward the position of this isosbestic point as a result of a hypsochromic shift. A negative transient response developed between approximately 646 nm and beyond the upper detection limit of the probe at 870 nm (Fig. 3(a), and Fig. S16). This negative response rose and decayed in parallel with the ESA and was connected to it *via* the aforementioned isosbestic point. As indicated by the inverted absorption spectrum (Fig. 3(a), grey) and given that ICG emits only at longer wavelengths around 800 nm in water, the negative transient response was attributed to ground-state bleaching (GSB) and stimulated emission (SE) was not considered below 800 nm, in agreement with the transient measurements of ICG in EtOH and DMSO (SI), as well as with previous reports.[15] An isosbestic point with a negative pump-induced ΔOD appeared at ~684 nm within the first 9 ps, bathochromically shifted relative to that on the baseline and exhibiting a formation timescale comparable to that observed in EtOH and DMSO. In contrast, in these solvents the isosbestic point appeared at ΔmOD > 0 and was hypsochromically shifted relative to that on the baseline (SI), indicating a divergent photophysical process. The transient response in water decayed completely within approximately 500 ps, whereas in EtOH and DMSO it remained detectable beyond the maximum probed delay time of 1 ns. Consequently, the relaxation dynamics of photoexcited ICG in aqueous environments were classified as significantly faster.

Similar to the stationary spectra, the transient response in water exhibits a pronounced concentration dependence (Fig. 3, and Fig. S17). Especially at early delay times, the spectral shape evolved from a single global maximum at ~570 nm (c_{ICG} = 10 μM) to a dual-band ESA with an emerging second peak at ~540 nm at higher concentrations. This maximum became more pronounced with increasing ICG concentration. In parallel, the GSB region develops an additional hypsochromically shifted minimum that grows in intensity and shifts progressively to shorter wavelengths with increasing concentration, matching the absorption maximum of the aggregated ICG species in the steady-state absorption spectra, as confirmed by the inverted steady-state absorption spectra (grey). Both modifications in the transient-absorption band shapes are likely attributable to aggregation-induced additional absorption bands in the steady-state absorption spectra. Accordingly, the maximum of the ESA at 570 nm and the minimum of the GSB around 750 nm were assigned to monomeric ICG, while the

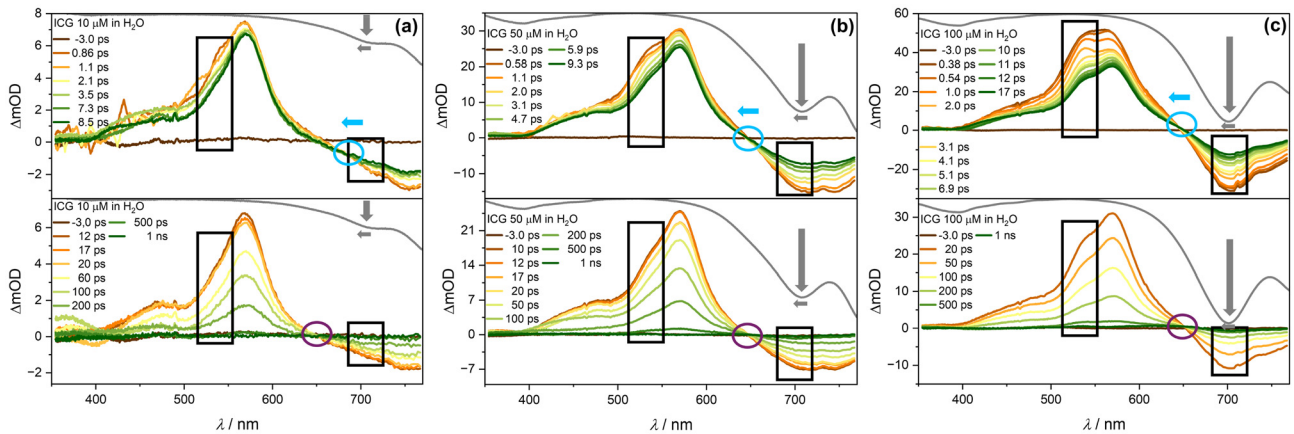

Fig. 3 TAS of ICG in H_2O at delay times as indicated. (a) c_{ICG} = 10 μM, $OD_{800\ nm}$ = 0.0623, (b) c_{ICG} = 50 μM, $OD_{800\ nm}$ = 0.2503, (c) c_{ICG} = 100 μM, $OD_{800\ nm}$ = 0.4252. λ_{ex} = 800 nm, E_{ex} = 1.0 μJ. The blue circles mark the isosbestic points at (a) 684 nm, (b) 648 nm and (c) 640 nm. The violet circles indicate the isosbestic points at (a) 646 nm, (b) 645 nm and (c) 652 nm. The blue arrow indicates the direction of the shift of the isosbestic point (blue) with increasing concentration. The black rectangle highlights the area in which band signatures showed concentration-dependent modifications. The steady-state absorption spectra (grey) are shown in the upper part of the TAS with an inverted, non-displayed OD axis. The grey arrows illustrate the concentration-dependent changes in the steady-state absorption spectra. Path length 1 mm.

maximum of the ESA around 540 nm and the hypsochromically shifted minimum of the GSB were attributed to ICG dimers and oligomers. At short delay times (<20 ps), the isosbestic point underwent a hypsochromic shift from 684 nm for the 10 μM solution to 648 nm at 50 μM and further to approximately 640 nm for the 100 μM ICG solution, accompanied by a change in ΔmOD. In contrast, the isosbestic point obtained at longer delay times (violet circle) remained essentially unchanged in position.

Given the coexistence of multiple ICG species in water even at the lowest resolvable concentration, we employed a parallel global analysis using decay-associated difference spectra (DADS) to extract the time constants and spectral signatures of the individual processes without assuming sequential decay pathways that cannot be resolved under the present experimental conditions (Fig. 4). Since this analysis is based on simulations rather than on detailed kinetic modelling, the extracted time constants likely represent a superposition of multiple relaxation pathways such as IC, IVR/VR (intramolecular vibrational redistribution/vibrational relaxation) and fluorescence. While a more refined modelling approach combined with selective excitation of individual ICG species at distinct probe wavelengths could further disentangle these contributions, the applied method provides a sufficient framework for identifying the processes within the scope of this study.

Fig. 4 presents the DADS of ICG in aqueous solution across a concentration range from 10 to 100 μM. Although the timescale of τ_1 of ICG in water (1–10 ps) was similar in magnitude to that in EtOH and DMSO, the corresponding amplitude spectrum A_1 (black) showed pronounced spectral deviations, pointing to distinct excited-state relaxation pathways. The band shape attributed to ICG aggregates in the TAS as a function of concentration (Fig. 3) resemble the signature of A_1 (grey) in the DADS spectra (Fig. 4, and Fig. S18). For ICG solutions with concentrations up to 50 μM, A_1 featured a maximum at approximately 535 nm. The isosbestic point of A_1 shifted toward shorter wavelengths with increasing concentration, in line with the isosbestic point observed in the TAS at early delay times (<20 ps). Given that the spectral characteristics of A_1 scaled with ICG concentration and were absent in EtOH and DMSO, this component was assumed to reflect the aggregation behaviour of ICG. Accordingly, A_1 described the depopulation of the S_1 state of ICG H-aggregates in the probe range from 400 nm up to the isosbestic point and the subsequent population of the S_0 state beyond it. Triplet-state dynamics within the short delay range below 10 ps were deemed unlikely given that literature-reported values[37,49] are substantially longer. In one report,[27] the formation of the triplet state from the first excited singlet state of ICG in aqueous solution is considered negligible and thus an assignment of τ_1 to triplet-state dynamics of ICG in water was not further pursued. Consistent with observations in EtOH and DMSO (SI), the spectral features of A_2 closely resembled those of the transient response at later delay times (>10 ps). The spectral region and intensity maximum of the ESA coincided with the decaying component, while the region of the GSB corresponded to the rising process of A_2. Both processes were connected *via* an isosbestic point, whose position aligned with that of the isosbestic point at ΔmOD = 0 in the TAS. These observations indicate that the S_1–S_0 relaxation dynamics of ICG in aqueous solution are represented by A_2 and can therefore be attributed to τ_2 (120–160 ps). τ_2 closely matched the fluorescence lifetime determined by TCSPC (Fig. S12) and literature-reported values[15] for the lifetime of the S_1 state of ICG in aqueous solution, thereby supporting its assignment to the first excited singlet state. In aqueous solution, the S_1 state lifetime of ICG was reduced by a factor of approximately five compared to EtOH (500–600 ps) and by a factor of nine relative to DMSO (700–900 ps) (SI). This trend was consistent with the fQY measured in the three solvents by steady-state fluorescence spectroscopy, indicating a correlation between the S_1 state lifetime and the fQY across all solvents.

The determined time constants τ_1 and τ_2 showed no significant differences across the investigated concentration range (Fig. 4). Within this concentration range, the predominated species of the H-aggregates was assumed to be the ICG dimer, characterised by a lifetime of the first excited singlet state on the order of a few ps (τ_1), whose relative abundance increased with rising ICG concentration. This observation was further supported by the amplitude ratio of A_2 to A_1, which progressively declined from 4.9 at 10 μM to 1.7 at 100 μM as the concentration increased (Fig. 4). Within the region of the GSB, A_1 displayed a pronounced minimum at 700 nm for the 100 μM solution. As previously noted for the steady-state absorption spectra, this feature is characteristic for oligomeric ICG struc-

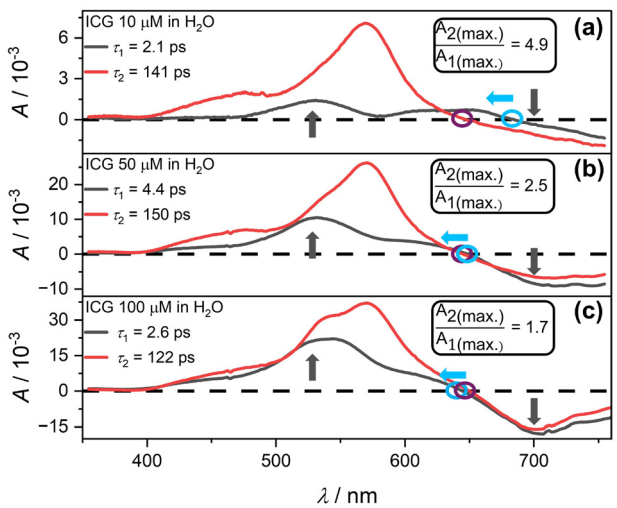

Fig. 4 DADS spectra of ICG in H_2O along with associated time constants τ_1 and τ_2. (a). c_{ICG} = 10 μM, $OD_{800\ nm}$ = 0.0623, (b) c_{ICG} = 50 μM, $OD_{800\ nm}$ = 0.2503, (c) c_{ICG} = 100 μM, $OD_{800\ nm}$ = 0.4252. λ_{ex} = 800 nm, E_{ex} = 1.0 μJ. The blue circles mark the isosbestic points at (a) 684 nm, (b) 648 nm and (c) 640 nm. The violet circles indicate the isosbestic points at (a) 646 nm, (b) 645 nm and (c) 652 nm. Changes in the amplitude spectrum A_1 (grey) with increasing concentration are illustrated by grey arrows. The blue arrow indicates the direction of the shift of the isosbestic point (blue) with increasing concentration. The amplitude ratios of A_2 and A_1 at their respective maxima are provided.

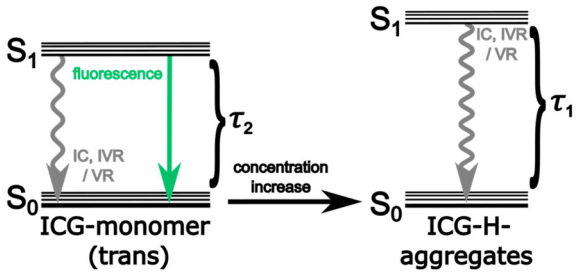

Fig. 5 Proposed relaxation dynamics of ICG in aqueous solution following photoexcitation at 800 nm. The S_1 state of the *trans*-isomer of monomeric ICG decays within τ_2 *via* a combination of IC and IVR/VR as well as fluorescence. The S_1 dynamics of monomeric ICG are superimposed by the S_1 dynamics of dimers and oligomers, which are collectively summarised as H-aggregates. The decay of the S_1 state in H-aggregates occurs within τ_1 predominantly *via* a combination of IC and IVR/VR (grey arrow) and not *via* fluorescence. Adapted from ref. 14 and 26.

tures. Accordingly, the depiction of oligomer dynamics in the TAS of the 100 μM ICG solution is plausible. It was assumed that their TAS reflected a superposition of the dynamics of multiple species, including contributions from monomeric, dimeric and oligomeric forms of the dye. This further accounts for the enhanced prominence of a shoulder around 535 nm in A_2 associated with increasing concentration. Previous studies[26,27] have demonstrated that ICG H-aggregates function as non-emissive fluorescence quenchers of ICG monomers.[27] The QY of IC for ICG in aqueous solution has been reported to be approximately 85%,[21] which was further increased to nearly 96% by Li *et al.*[14] through the synthesis of covalently linked ICG dimers. Consequently, IC is considered the main factor determining the observed lifetime of the S_1 state of ICG dimers and oligomers. No significant variation was observed in the lifetime of the ICG monomer or in the characteristic band shape across the entire range of tested concentrations (Fig. 3 and 4). Only at concentrations of 50 μM and above the H-aggregates affected the amplitude spectrum associated with the S_1–S_0 dynamics of the ICG monomer (A_2), evidenced by the emergence of a shoulder near 535 nm. An increase in concentration showed no significant effect on either the time constant τ_2 or the spectral structure of A_2. Therefore, the lifetime of S_1 of ICG in water was classified as concentration-independent within the examined range. This observation is supported by the study of Gerega *et al.*,[35] who reported only minor differences in the fluorescence lifetime of ICG in water at varying concentrations. The proposed relaxation mechanism of ICG in water is illustrated in Fig. 5.

Conclusions

The photophysical behaviour of ICG in the condensed phase was investigated as a function of concentration in the solvents EtOH, DMSO and water, providing a foundation for elucidating its photophysical properties within inorganic ICG-containing NPs. In EtOH and DMSO, the steady-state absorption spectra of ICG displayed concentration-independent band shapes within the investigated range and conformed the linear scaling predicted by the Beer–Lambert law. In contrast, in aqueous solution, concentration-dependent aggregation of ICG significantly influenced the absorption behaviour, leading to deviations from the linearity of the Beer–Lambert law and the appearance of an addition, hypsochromic absorption maximum. The S_1 lifetime of ICG was determined to be in the range of 120 to 160 ps in aqueous solution, of 500 to 600 ps in EtOH and of 700 to 900 ps in DMSO, showing no concentration dependence. In agreement with previous studies,[37] it was further demonstrated that the lifetime of the first excited state of ICG decreases with increasing solvent polarity. The fQY was quantified using steady-state fluorescence spectroscopy. It was found to be approximately five times higher in EtOH and about nine times higher in DMSO compared to water, where it measured around 5% for diluted solutions below 0.3 μM. These results indicate a correlation between the fQY and the lifetime of the first excited singlet state across the three solvents. Based on previous studies,[21] IC is considered the dominant relaxation pathway of the S_1 state of ICG. Accordingly, the S_1 lifetime was assumed to be primarily governed by IC and fluorescence. In aqueous solution, the transient response decayed completely within approximately 500 ps, whereas in EtOH and DMSO it persisted beyond 1 ns, indicating the presence of a longer-lived state or species in these solvents. A dynamic component with a time constant of less than 10 ps was identified in water and its intensity increased with rising ICG concentration. This ultrafast process was assigned to the S_1 lifetime of ICG H-aggregates. At a concentration of 100 μM, the observed dynamics reflected a superposition of various dynamics originating from multiple ICG species, including monomers, dimers and oligomers. Given that H-aggregates serve as non-emissive fluorescence quenching centres for monomeric ICG and primarily relax to the ground state *via* IC,[14,21] it was inferred that the overall QY of IC increases with concentration in the mixed-species system, while any resulting changes in the characteristic time constants remain within the limits of the measurement uncertainty.

Due to the high QY of IC during the relaxation from the S_1 state to the ground state in ICG H-aggregates and the associated increased heat generation, combined with the ability of NPs to promote enhanced formation of ICG aggregates and thereby amplify photothermal effects,[7] we consider ICG-NPs to hold promising potential for photothermal applications. However, further extensive investigations are required to elucidate the dynamics of ICG within the ICG-containing NPs, with particular consideration of the dye concentration and the solvent environment.

Materials and methods

Stationary spectra

Stationary absorption spectra including baseline subtraction were obtained using a CaryWin500 from Varian (Agilent

Technologies, Waldbronn, Germany) at a wavelength interval of 1 nm in cuvettes with path lengths of 1 mm and 1 cm from Spectrosil (Starna GmbH, Pfungstadt, Germany).

Fluorescence spectra were recorded with a FluoroMax 4 (Horiba, Oberursel, Germany) with excitation wavelengths of 366 nm, 720 nm and 750 nm and varying slit widths. The slit width for each measurement is noted accordingly. The temperature was maintained at 20° C using a thermostat.

The emission measurements and the determination of the fQY were performed based on the protocol described by Resch-Genger *et al.*[46] The fQY of the fluorophore was assessed by comparison with a reference system of reliably known fQY under identical experimental conditions.[46,50,51] Suitable standards considered reliable or previously studied by multiple independent groups were reviewed within the framework of the IUPAC project. no. 2004-021-1-300,[50] which recommended HITCI as a reference for fQY determination of ICG.[46,50] To further reduce potential errors, IR-820 in MeOH was used in parallel to HITCI in EtOH (Fig. S6). To ensure spectral coverage of the reference dyes and excitation near the absorption maximum of ICG, HITCI was excited at 700 nm, while IR-820 in MeOH was excited at 750 nm. Since differing excitation wavelengths can introduce further uncertainty due to variation in relative photon flux,[50] identical excitation wavelengths were employed for both sample and reference. As high dye concentrations may cause significant deviations in fQY due to inner filter and reabsorption effects,[52] fQY were comprehensively determined in a concentration-dependent manner for all systems (Tables S1–S8). Following recommendations by Resch-Genger *et al.*,[46] all values were validated by independent replicate measurements. Literature values for reference fQYs were selected with particular attention to studies involving concentration-dependent emission measurements.[42,43,53] As the fQYs obtained for ICG were consistent across both excitation wavelengths and no wavelength-dependent variations in spectral band shape or peak position were observed (Tables S3–S8), the discussion is based on the measurements acquired at 750 nm (Fig. 2(c, d) and Fig. S1(b)), which is closer to the main absorption band of ICG. The fQY Φ was calculated based on the emission spectra following the procedure established by Demas and Crosby (eqn (1)).[43,46,54]

$$\Phi_{f,x} = \Phi_{f,\mathrm{st}} \frac{F_x f_{\mathrm{st}}(\lambda_{\mathrm{ex,st}})}{F_{\mathrm{st}} f_x(\lambda_{\mathrm{ex},x})} \frac{{n_x}^2}{{n_{\mathrm{st}}}^2} \frac{q_{\mathrm{p,st}}(\lambda_{\mathrm{ex,st}})}{q_{\mathrm{p},x}(\lambda_{\mathrm{ex},x})} \quad (1)$$

The indices x and st correspond to the sample and the standard, while f and ex denote fluorescence and excitation wavelength. F represents the integrated spectral fluorescence photon flux over the full emission range of the dye. Photon fluxes at the sample position corresponding to the standard and the sample at their respective excitation wavelengths are indicated by $q_{\mathrm{p,\ st}}$ and $q_{\mathrm{p,x}}$, respectively. In cases where the standard and the sample are excited at the same wavelength, the photon fluxes are equal.[54] The parameter f refers to the fraction of excitation light absorbed by the chromophore, which is derived from the absorption spectrum as described in eqn (2).[43,46]

$$f(\lambda_{\mathrm{ex}}) = 1\text{–}10^{-\mathrm{OD}(\lambda_{\mathrm{ex}})} \quad (2)$$

To assess the impact of reabsorption on the emission spectra, they were further corrected using eqn (3) and (4).[55]

$$I_{\mathrm{f}}(\lambda_{\mathrm{em}}) = {I_{\mathrm{f}}}^0(\lambda_{\mathrm{em}})P \quad (3)$$

$I_{\mathrm{f}}(\lambda_{\mathrm{em}})$ and ${I_{\mathrm{f}}}^0(\lambda_{\mathrm{em}})$ represent the corrected and measured luminescence intensity, respectively, while P accounts for the correction of the reabsorption (eqn (4)).[55]

$$P = (1+k)\frac{1-\exp(-2.3\mathrm{OD}(\lambda_{\mathrm{ex}}))}{1-\exp(-2.3(\mathrm{OD}(\lambda_{\mathrm{ex}})+\mathrm{OD}(\lambda_{\mathrm{em}})))} \quad (4)$$

The indices ex and em denote the absorbing and emitting wavelength and $k = \mathrm{OD}(\lambda_{\mathrm{em}})/\mathrm{OD}(\lambda_{\mathrm{ex}})$. It should be noted that eqn (4) is only valid when the beam enters and exits the cuvette perpendicularly.[55]

TCSPC

TCSPC spectra were acquired using a Spex Fluorofog3 (Horiba, Oberursel, Germany) in cuvettes with path lengths of 1 cm from Spectrosil (Starna GmbH, Pfungstadt, Germany). NanoLED 366 was used for excitation with a pulse duration of 1.2 ns, a repetition rate of 1 MHz and a middle energy of 4 pJ. The probe wavelength was 810 nm.

Excitation in the NIR proved impractical for ICG due insufficient photon count rates. Consequently, ICG was excited at its local absorption maximum at 366 nm. No significant differences were observed between the stationary emission spectra of ICG upon excitation at 366 nm and 750 nm (Fig. S8–S10).

Transient-absorption spectra

The methodology for transient-absorption spectroscopy has been described in detail in previous reports.[56] In essence, a Ti: sapphire laser system (Astrella, Coherent, Utrecht, The Netherlands, 800 nm, 1 kHz, 35 fs, 7.2 mJ) was used to generate the pulses for both excitation and probing. For excitation, the fundamental of the laser system was used. A white light continuum spanning 350–750 nm and 400–900 nm was generated by irradiating a continuously moving CaF_2 crystal. The white light was divided into probe and reference beams. The probe beam was spatially and temporarily overlapped with the pump pulse in the sample (Starna cuvette, Suprasil quartz, optical path length of 1 mm), which was continuously stirred using a miniaturised magnetic bar. Pump-induced changes were recorded by a CCD camera (Linescan Series2000, 512 pixels, Si detector, Entwicklungsbüro Stresing, Berlin, Germany). The reference pulse was simultaneously detected by an additional, identical CCD camera. Spectral dispersion of the white light prior to detection was achieved using a prism with an average resolution of approximately 1.5 nm. For the probing in the spectral range from 400–900 nm, further conditioning of the white light was required. To avoid a saturation of the CCD cameras, the intensity of the 800 nm component

was attenuated using a bandpass filter (BG38) positioned in the probe beam path upstream of the sample. BG18 bandpass filters were placed in front of both CCD cameras for the spectral range of 350–750 nm. Owing to their limited transmission in the NIR region, these filters were substituted with BG63 bandpass filters when extending the probe range to 400–900 nm.

Data processing was performed with an in-house written LabView program. An optical chopper (Thorlabs, Bergkirchen, Germany) was employed to block every second pump pulse, enabling the acquisition of differential optical density spectra (ΔOD) by comparing spectra with and without excitation. Temporal broadening of the pulses was induced by the optical components of the transient spectrometer and the transmission through the glass cuvette containing the sample. The resulting group velocity mismatch in the TAS was corrected prior to data analysis using an in-house written program developed in Wolfram Mathematica, utilizing a Sellmeier[57] plot. The time constants and the DADS associated with the individual relaxation processes of the sample were extracted by globally fitting the function defined in eqn (5)[58] to the transient response, using an in-house written MatLab script that employed the Nelder–Mead–Simplex algorithm.[59]

$$\Delta\mathrm{OD}(t) = \underbrace{\frac{1}{2}\left(1+\mathrm{erf}\left[\sqrt{4\cdot\ln(2)}\cdot\frac{t-x_0}{\tau_0}\right]\right)}_{\text{(a)}} \times \underbrace{\sum_{i=1}^{n} A_i(\lambda)\cdot\exp\left(\frac{t-x_0}{\tau_i}\right)}_{\text{(b)}} \quad (5)$$

The rise time of the transient response (τ_0) represented the experimental time resolution. The temporal zero point (x_0) on the x-axis was set to approximately half of τ_0, provided that τ_0 was significantly shorter than the lifetime of the excited state. The number of exponential functions n necessary to achieve an adequate fit of eqn (5) to the experimental data varied according to the underlying dynamics of the system. From this fitting procedure, the time constants τ_i and corresponding amplitudes A_i of the individual processes i were obtained. Amplitude intensities varied with probe wavelength and were displayed as amplitude spectra in the DADS.[60] Each spectrum reflected a distinct dynamic, defined by its corresponding time constant. Positive amplitudes indicated decay processes, while negative amplitudes signified population rise. A transition between amplitudes of opposite sign, resulting in $A = 0$ at a specific probe wavelength, indicated an isosbestic point.

Sample preparation

Indocyanine green (Carl Roth, Karlsruhe, Germany) was dissolved in EtOH (Fisher Scientific, Schwerte, Germany, ≥99.8%), DMSO (Carl Roth, Karlsruhe, Germany, ≥99.5%) and demineralised water (pH = 5). HITCI (Radiant Dyes, Wermelskirchen, Germany) and IR-820 (Sigma Aldrich, Taufkirchen, Germany) were dissolved in EtOH (Fisher Scientific, Schwerte, Germany, ≥99.8%) and MeOH (Sigma Aldrich, Taufkirchen, Germany, ≥99.9%). Fluorescence measurements of the dye solutions were performed following the protocol by Resch-Genger *et al.*[46] As reported by Resch-Genger *et al.*,[46] the presence of oxygen has negligible effect on the fQY and fluorescence lifetimes if the fluorescence lifetime is below 10 ns. Given that the chromophores investigated in this study exhibit lifetimes well below this threshold,[61–64] fluorescence measurements of the dye solutions were performed without prior deoxygenation to ensure comparability with literature data obtained under similar conditions. To minimise potential photoinduced degradation of ICG caused by reactions with oxygen under relatively high irradiation intensities and prolonged measurement durations of approximately 17 min during transient measurements, the samples were purged with nitrogen gas (Air Liquide, 99.99%) for 10 min prior to data acquisition. To monitor degradation following photoexcitation, steady-state absorption spectra of the samples were recorded both before and after the transient-absorption measurements (Fig. S11).

Conflicts of interest

There are no conflicts to declare.

Data availability

The data supporting this article have been included as part of supplementary information (SI). The SI provides information of additional Steady-state absorption and fluorescence spectra, TCSPC measurements, Transient absorption spectra as well as Notes and references. See DOI: **https://doi.org/10.1039/d5dt01894c**.

Acknowledgements

We acknowledge continued key support from the Karlsruhe Institute of Technology (KIT).

References

1 M. Khorenko, J. Pfeifer, J. Napp, A. Meschkov, F. Alves, U. Schepers and C. Feldmann, *J. Mater. Chem. B*, 2023, **11**, 3635–3649.
2 M. Poß, R. J. Tower, J. Napp, L. C. Appold, T. Lammers, F. Alves, C.-C. Glüer, S. Boretius and C. Feldmann, *Chem. Mater.*, 2017, **29**, 3547–3554.
3 P. Neidinger, J. Davis, D. Voll, E. A. Jaatinen, S. L. Walden, A. N. Unterreiner and C. Barner-Kowollik, *Angew. Chem., Int. Ed.*, 2022, **61**, e202209177.
4 A. H. Bonardi, F. Bonardi, F. Morlet-Savary, C. Dietlin, G. Noirbent, T. M. Grant, J. P. Fouassier, F. Dumur,

B. H. Lessard, D. Gigmes and J. Lalevée, *Macromolecules*, 2018, **51**, 8808–8820.
5 E. D. Cosco, I. Lim and E. M. Sletten, *ChemPhotoChem*, 2021, **5**, 727–734.
6 H. K. Yoon, A. Ray, Y.-E. K. Lee, G. Kim, X. Wang and R. Kopelman, *J. Mater. Chem. B*, 2013, **1**, 5611–5619.
7 X. Sun, Y. Peng, P. He, H. Cheng, D. Li, H. Liu, H. Lin and G. Liu, *Nanoscale*, 2024, **16**, 11411–11428.
8 C. Egloff-Juras, L. Bezdetnaya, G. Dolivet and H.-P. Lassalle, *Int. J. Nanomed.*, 2019, 7823–7838.
9 M. H. Abdel-Kader, *Photodynamic Therapy: From Theory to Application*, Springer, Berlin, Heidelberg, 2014.
10 A. Fernandez-Fernandez, R. Manchanda, T. Lei, D. A. Carvajal, Y. Tang, S. Z. R. Kazmi and A. J. McGoron, *Mol. Imaging*, 2012, **11**, 99–113.
11 A. M. Gamal-Eldeen, L. M. Fouad, S. M. El-Daly, E. A. El-Hussieny and E. S. E. Denshary, *Photodiagn. Photodyn. Ther.*, 2014, **11**, 239–249.
12 C. S. Shemesh, C. W. Hardy, D. S. Yu, B. Fernandez and H. Zhang, *Photodiagn. Photodyn. Ther.*, 2014, **11**, 193–203.
13 C. Wang, H. Tao, L. Cheng and Z. Liu, *Biomaterials*, 2011, **32**, 6145–6154.
14 L. Li, N. E. I. Guissi, Y. Peng, S. Nie, H. Cai, C. J. Butch and Y. Wang, *Cell Rep. Phys. Sci.*, 2024, **5**, 101748.
15 K. Liao, Y. Pan, Z. Wu, W. Yao, X. Miao, X. Lu, Q. Fan and W. Hu, *Chem. – Asian J.*, 2022, **17**, e202200112.
16 B. L. Neumeier, M. Khorenko, F. Alves, O. Goldmann, J. Napp, U. Schepers, H. M. Reichardt and C. Feldmann, *ChemNanoMat*, 2019, **5**, 24–45.
17 F. Yan, H. Wu, H. Liu, Z. Deng, H. Liu, W. Duan, X. Liu and H. Zheng, *J. Controlled Release*, 2016, **224**, 217–228.
18 C.-K. Lim, J. Heo, S. Shin, K. Jeong, Y. H. Seo, W.-D. Jang, C. R. Park, S. Y. Park, S. Kim and I. C. Kwon, *Cancer Lett.*, 2013, **334**, 176–187.
19 G. M. F. Calixto, J. Bernegossi, L. M. d. Freitas, C. R. Fontana and M. Chorilli, *Molecules*, 2016, **21**, 342.
20 Y. Cai, T. Chai, W. Nguyen, J. Liu, E. Xiao, X. Ran, Y. Ran, D. Du, W. Chen and X. Chen, *Signal Transduction Targeted Ther.*, 2025, **10**, 115.
21 S. Houthoofd, M. Vuylsteke, S. Mordon and I. Fourneau, *Photodiagn. Photodyn. Ther.*, 2020, **29**, 101568.
22 M. Poß, E. Zittel, A. Meschkov, U. Schepers and C. Feldmann, *Bioconjugate Chem.*, 2018, **29**, 2818–2828.
23 C. Feldmann, *Z. Anorg. Allg. Chem.*, 2022, **648**, e202200062.
24 C. Ritschel, J. Napp, F. Alves and C. Feldmann, *Nanoscale*, 2022, **14**, 16249–16255.
25 L. d. Boni and C. R. Mendonça, *J. Phys. Org. Chem.*, 2011, **24**, 630–634.
26 B. Chon, W. Ghann, J. Uddin, B. Anvari and V. Kundra, *Int. J. Mol. Sci.*, 2023, **24**, 13030.
27 R. Philip, A. Penzkofer, W. Bäumler, R. M. Szeimies and C. Abels, *J. Photochem. Photobiol., A*, 1996, **96**, 137–148.
28 D.-H. Li and B. D. Smith, *Chem. – Eur. J.*, 2021, **27**, 14535–14542.
29 F. Rüttger, S. Mindt, C. Golz, M. Alcarazo and M. John, *Eur. J. Org. Chem.*, 2019, 4791–4796.
30 B. Jung, V. I. Vullev and B. Anvari, *IEEE J. Sel. Top. Quantum Electron.*, 2013, **20**, 149–157.
31 P. Elliott, K. Burke and F. Furche, *Rev. Comput. Chem.*, 2008, **26**, 91–165.
32 R. Malallah, G. Gallagher, N. Hardy, J. Dalli, D. Wu, D. F. O'Shea, J. Sheridan and R. Cahill, *Proc. SPIE*, 2022, **12146**, 1214608.
33 V. Saxena, M. Sadoqi and J. Shao, *J. Pharm. Sci.*, 2003, **92**, 2090–2097.
34 K. Urbanska, B. Romanowska-Dixon, Z. Matuszak, J. Oszajca, P. Nowak-Sliwinska and G. Stochel, *Acta Biochim. Pol.*, 2002, **49**, 387–391.
35 A. Gerega, N. Zolek, T. Soltysinski, M. Daniel, S. Piotr, T. Beata and L. Adam, *J. Biomed. Opt.*, 2011, **16**, 067010.
36 J. Zhou, X. Fan, D. Wu, J. Liu, Y. Zhang, Z. Ye, D. Xue, M. He, L. Zhu and Z. Feng, *Light: Sci. Appl.*, 2021, **10**, 182.
37 L. De Boni, D. C. J. Rezende and C. R. Mendonça, *J. Photochem. Photobiol., A*, 2007, **190**, 41–44.
38 J. F. Zhou, M. P. Chin and S. A. Schafer, *Proc. SPIE*, 1994, **2128**, 495–505.
39 M. Mauerer, A. Penzkofer and J. Zweck, *J. Photochem. Photobiol., B*, 1998, **47**, 68–73.
40 F. Rotermund, R. Weigand and A. Penzkofer, *Chem. Phys.*, 1997, **220**, 385–392.
41 R. C. Benson and H. A. Kues, *J. Chem. Eng. Data*, 1977, **22**, 379–383.
42 C. Würth, J. Pauli, C. Lochmann, M. Spieles and U. Resch-Genger, *Anal. Chem.*, 2012, **84**, 1345–1352.
43 K. Rurack and M. Spieles, *Anal. Chem.*, 2011, **83**, 1232–1242.
44 R. Benson and H. Kues, *Phys. Med. Biol.*, 1978, **23**, 159.
45 S. A. Soper and Q. L. Mattingly, *J. Am. Chem. Soc.*, 1994, **116**, 3744–3752.
46 U. Resch-Genger and K. Rurack, *Pure Appl. Chem.*, 2013, **85**, 2005–2013.
47 R. Hoshi, K. Suzuki, N. Hasebe, T. Yoshihara and S. Tobita, *Anal. Chem.*, 2020, **92**, 607–611.
48 J. Maillard, K. Klehs, C. Rumble, E. Vauthey, M. Heilemann and A. Fürstenberg, *Chem. Sci.*, 2021, **12**, 1352–1362.
49 S. Reindl, A. Penzkofer, S. H. Gong, M. Landthaler, R. M. Szeimies, C. Abels and W. Bäumler, *J. Photochem. Photobiol., A*, 1997, **105**, 65–68.
50 A. M. Brouwer, *Pure Appl. Chem.*, 2011, **83**, 2213–2228.
51 C. Würth, M. G. González, R. Niessner, U. Panne, C. Haisch and U. R. Genger, *Talanta*, 2012, **90**, 30–37.
52 L. V. Ferreira and S. M. Costa, *J. Lumin.*, 1991, **48**, 395–399.
53 N. S. James, Y. Chen, P. Joshi, T. Y. Ohulchanskyy, M. Ethirajan, M. Henary, L. Strekowsk and R. K. Pandey, *Theranostics*, 2013, **3**, 692–702.
54 C. Würth, M. Grabolle, J. Pauli, M. Spieles and U. Resch-Genger, *Anal. Chem.*, 2011, **83**, 3431–3439.
55 J. Grzywacz and T. Zaleski, *J. Lumin.*, 1984, **29**, 235–238.
56 N. C. Michenfelder, C. Gienger, M. Dilanas, A. Schnepf and A.-N. Unterreiner, *Molecules*, 2020, **25**, 2639.
57 W. Sellmeier, *Ann. Phys.*, 1871, **219**, 272–282.
58 S. Pedersen and A. H. Zewail, *Mol. Phys.*, 1996, **89**, 1455–1502.

59 J. C. Lagarias, J. A. Reeds, M. H. Wright and P. E. Wright, *SIAM J. Optim.*, 1998, **9**, 112–147.
60 I. H. M. van Stokkum, D. S. Larsen and R. van Grondelle, *Biochim. Biophys. Acta, Bioenerg.*, 2004, **1657**, 82–104.
61 D. K. Das, K. Makhal, S. Singhal and D. Goswami, *Chem. Phys. Lett.*, 2013, **579**, 45–50.
62 A. Bera, M. N. Hasan, U. Pal, D. Bagchi, T. K. Maji, T. Saha-Dasgupta, R. Das and S. K. Pal, *J. Photochem. Photobiol., A*, 2022, **424**, 113610.
63 K. C. Jena and P. B. Bisht, *Chem. Phys.*, 2005, **314**, 179–188.
64 A. Bera, D. Bagchi and S. K. Pal, *J. Photochem. Photobiol., A*, 2019, **123**, 7550–7557.